Resonance ionization of zirconium

R. Trappitsch[1,3] · D. Z. Shulaker[2] · W.-J. Ong[2] · M. R. Savina[2] · B. H. Isselhardt[2]

Abstract

Measuring the isotopic composition of trace Zr in presolar stardust grains allows us to study the environment of slow neutron-capture nucleosynthesis in asymptotic giant branch stars. Here, we present a newly characterized Zr resonance ionization scheme that can be saturated with state-of-the-art titanium-sapphire lasers and yields a useful yield of $(5.4 \pm 0.4)\%$. Resonance ionization is achieved in two steps: after first being excited with a photon at 319.215 nm, neutral Zr atoms are then ionized with a photon at 388.988 nm, where both wavelengths are reported as in vacuum.

Introduction

Presolar grains, or "stardust" particles that are retrieved from meteorites [1], condensed in the outflows of dying stars and thus their isotopic composition recorded their parent stars' nucleosynthetic fingerprint. Acid-resistant presolar phases, such as silicon carbide (SiC), are removed from their meteoritic host by acid-separation, which is generally followed by acid cleaning of the grains' surfaces to remove any residual meteoritic contamination. Analyses of these cleaned micrometer-sized particles yield valuable insights into stellar nucleosynthesis and galactic chemical evolution. However, due to the small size of these grains (of order µm), trace element isotopic analyses of presolar grains require suitable mass spectrometry techniques such as resonance ionization mass spectrometry (RIMS), which is capable of detecting atoms that only occur in trace amounts. RIMS is therefore ideally suited to analyze these atom-limited stardust grains. Most presolar SiC grains originate in asymptotic giant branch stars that are up to a few times the mass of the Sun. These stars are the hosts of the slow neutron-capture process (also known as the *s*-process) and produce about half the abundance of elements between Sr and Pb. "Slow" neutron-capture refers to the case when neutron capture produces a β^--unstable nucleus, which subsequently decays to its stable daughter prior to capturing another neutron. However, branch points exist where the β^--unstable nucleus has a long enough half-life that even slow neutron capture may be competitive with β^--decay. One such nucleus is ^{95}Zr, which has a half-life of 64 days. Neutron capture on ^{95}Zr yields ^{96}Zr, a stable nucleus. Analyzing the Zr isotopic composition of presolar grains thus enables studying the neutron flux in a star during the *s*-process, which can be used as a sensitive thermometer to study stellar evolution [2–4]. Due to the low abundnace of Zr in presolar SiC grains and the presence of interfering isotopes such as ^{92,94,96}Mo and ^{96}Ru, RIMS is the only technique to date that has been used to successfully analyze individual stardust particles for their isotopic Zr composition.

Our recent efforts to analyze Zr isotopes in presolar grains using a previously published resonance ionization scheme [3] gave unsatisfying sensitivity, resulting in low Zr counts and hence large uncertainties. Here we present a newly characterized Zr resonance ionization scheme accessible by titanium-sapphire lasers.

✉ R. Trappitsch
reto.trappitsch@epfl.ch

1   Department of Physics, Brandeis University, 415 South St, Waltham, MA 02453, USA

2   Nuclear and Chemical Sciences Division, Lawrence Livermore National Laboratory, 7000 East Ave, L-231, Livermore, CA 94550, USA

3   Present Address: Laboratory for Biological Geochemistry, School of Architecture, Civil & Environmental Engineering, École Polytechnique Fédérale de Lausanne, 1015 Lausanne, Switzerland

Experimental

All measurements presented here were performed on high-purity Zr foil. RIMS analyses were performed using the Laser Ionization Of Neutrals (LION) mass spectrometer at Lawrence Livermore National Laboratory. An overview of RIMS can be found in [5] and specific details on LION in [6]. In brief, Zr atoms were sputtered from the foil using a pulsed 15 keV Ga$^+$ beam at 60° incidence. For measurements, the ion beam was rastered over an area of ∼ 20 × 20 μm. Secondary ions created during the sputtering were cleared from the system by applying a brief voltage pulse to the sample, which effectively ejects them from the mass spectrometer. Neutral Zr atoms were then ionized using titanium-sapphire lasers specifically tuned to Zr resonance ionization transitions (Fig. 1). These photoions were then extracted, separated, and detected in a time-of-flight mass spectrometer. Arrival times of individual ions were recorded using a time-to-digital converter (FastComTec MCS 8a).

Results and discussion

Zirconium resonance ionization scheme

The Zr resonance ionization scheme determined in this work and detailed in the following sections is shown in Fig. 1. Neutral atoms in the $^3F_2$ ground state are excited to a $^3G_3$ state at 31,326.81 cm^{-1} [7] using a photon at 319.215 nm. From here, we performed a wavelength scan and detected
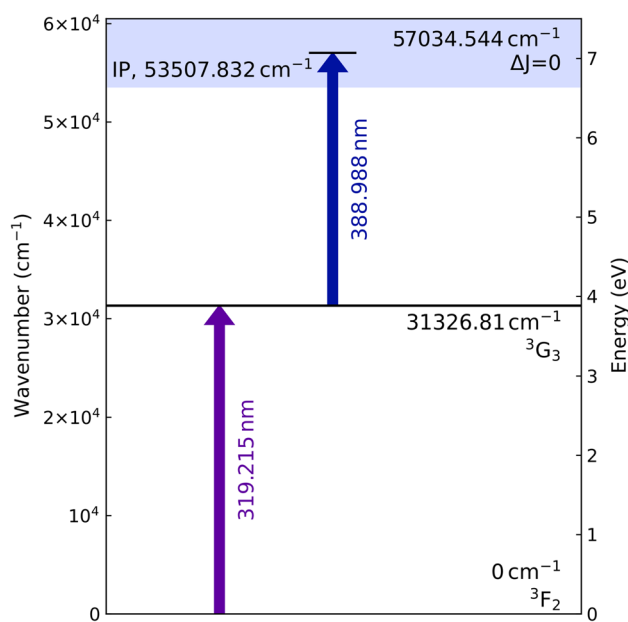
two autoionizing (AI) states above the ionization potential (IP). The state at 57,034.544 cm^{-1} shown in Fig. 1 was ultimately selected as superior for the reasons described below. Details on laser parameters for the selected scheme are given in Table 1. The Zr resonance ionization scheme presented is very similar to the one by [8]. These authors however provide no details about their scheme and the ionization wavelength they report is slightly different from the one determined in this work.

Wavelength scan of the ionization laser

To find a suitable ionization transition from the $^3G_3$ intermediate state, we performed a wavelength scan between 387.5 and 390.5 nm in steps of ∼ 50 pm. Note that all wavelengths in this manuscript are reported in vacuum. Previous work by our group indicates that this region should contain an autoionization transition. For each peak identified within a region, a finer wavelength scan in steps of ∼ 5 pm was conducted to determine the exact peak position and width of the transition.

Figure 2 shows all wavelength scan measurements for transitions originating from the $^3G_3$ intermediate state in the range 387.5–390.5 nm. Blue triangles represent the rough wavelength scan. Because the count rate slowly drifted over the measurement period, we applied a linear drift correction. The peak at 388.988 nm was measured in the beginning of the scan and at the end. Previous studies [9, 10] showed that these count rate drifts are due to re-oxidizataion of the surface and are mostly linear over the timescale of these scans. The first and last measurements at 388.988 nm were thus used to correct the acquired signal for count rate drifts. Red circles and green squares show the finer wavelength scans around the identified peak areas of interest.

The three scans shown in Fig. 2 were performed at different times. Therefore, each scan was normalized to its highest signal. Due to this normalization, the peak at 388.335 nm and 388.988 nm appear to have equal intensity, though this was not the case in absolute terms, which can be deduced from the difference in saturation power.

The ionization step reported by [8] is 388.86 nm (in vacuum). Figure 2 shows that the peak transition found in this work is 128 pm further to the red. Pellin and Nicolussi [8] do not discuss the details of their Zr resonance

Fig. 1 Zirconium resonance ionization scheme chosen in this work

Table 1 Characterization of the Zr resonance ionization lasers

Wavelength in vacuum (nm)	Pulse width (ns)	Bandwidth (nm)	Saturation irradiance (W cm^{-2})
319.215	13	∼ 3	1.54×10^3
388.988	14	∼ 5	1.98×10^4

Fig. 2 Wavelengths scanned for determining the wavelengths (shown in dashed lines) used in the Zr resonance ionization scheme
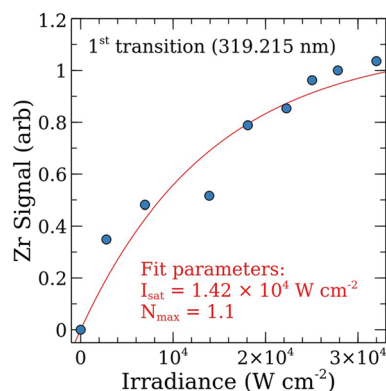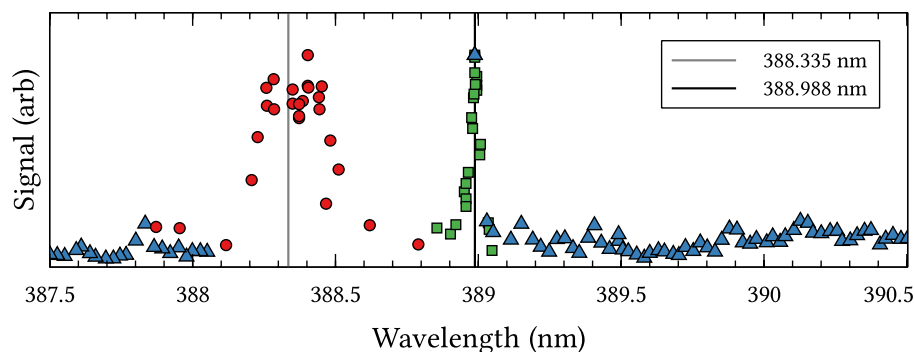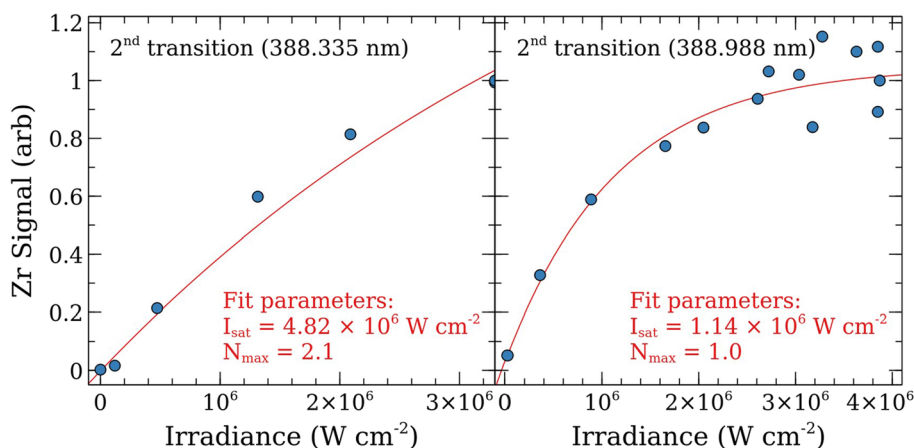

Fig. 3 Saturation curve measured for the first Zr resonance ionization transition at 319.215 nm

ionization scheme aside from presenting it in a figure. The origin of the difference compared to this work can therefore not be easily determined. One speculation is that a transition with a full-width at half maximum of < 10 pm is present at 388.86 nm. Our wavelength scan would not have found such a transition. However, such narrow transitions are generally not ideal for a stable ionization scheme, since small variations in laser wavelength would result in large signal fluctuations.

Saturation curves

An ideal ionization scheme requires, among other things, that (1) the transition can be easily saturated and (2) that the useful yield of the given transition is high. We record saturation curves for the resonance transition (Fig. 3) and for the two AI transitions (Fig. 4). These saturation curves show the signal level with respect to the irradiance of the laser transition of interest. The laser power for the transition under investigation was varied while the laser for the transition from the ground state to the intermediate state was held at constant power. Saturation curves are fitted with a first-order rate model [11]:

$$N = N_i + N_{max} \times \left[1 - \exp\left(\frac{-I}{I_{sat}}\right)\right] \quad (1)$$

where N_i is the signal at zero irradiance, N_{max} the maximum signal, I the laser irradiance, and I_{sat} the saturation irradiance of the transition. Note that the saturation irradiance in Eq. (1) corresponds to a signal level of ~ 63% of the maximum.

To account for variations in the amount of material sputtered from the Zr foil over time, the signal for each point in the saturation curve was corrected by bracketing with measurements made at standard laser powers. Figures 3 and 4

Fig. 4 Saturation curves for the two ionization wavelengths found by the wavelength scan (see Fig. 2). Only the transition at 388.988 nm could be saturated

show the saturation curves for the first resonance transition to the intermediate state, and the two AI transitions found during the wavelength scan, respectively. Parameters for the fit to Eq. (1) are given in the figures. Note that N_i is zero within uncertainties for all fits and is thus omitted.

Fitting Eq. (1) shows that the first resonance transition is saturated at an irradiance of 1.54×10^3 W cm^{-2} (Fig. 3). As seen in Fig. 4, only the AI transition at 388.988 nm could be saturated with our lasers. The saturation irradiance for this transition is 1.98×10^4 W cm^{-2}. The other, broader, ionization transition could not be saturated with our system. Our fit of Eq. (1) to the saturation curve estimates that a total irradiance of 8.36×10^4 W cm^{-2} would be required, and approximately half of the atoms are efficiently ionized at our maximum laser power. We therefore selected the transition at 388.988 nm as the preferred wavelength for Zr ionization.

Useful yield

Useful yield is defined as the number of ions detected divided by the number of atoms consumed during analysis. We standardized the conditions for ion detection as 10,000 measurements cycles (10 s @ 1 kHz) consisting of 300 ns Ga$^+$ pulses followed by resonanance ionization and detection. The number of Zr atoms consumed in a cycle is then determined by the Ga$^+$ current and the sputtering yield, s_y, which is the number of Zr atoms sputtered per Ga$^+$ atom incident on the surface. The useful yield is then given by:

$$UY = \frac{c \times q_e}{s_y \times \Delta t \times I \times n \times a_{Zr}} \tag{2}$$

where c is the number of Zr ions counted in n measurement cycles, q_e is the elementary charge, Δt is the Ga$^+$ pulse duration at a current of I. Finally, a_{Zr} is the Zr concentration of the sample surface. Gallium is implanted into the material during sputtering, thus lowering the Zr concentration. In equilibrium, the Zr surface concentration is expressed as

$$a_{Zr} = \frac{s_y}{1 + s_y}. \tag{3}$$

The Zr sputtering yield was determined by rastering the Ga$^+$ beam in continuous mode to sputter five $\sim 20 \times 20$ μm pits for five minutes each. The crater volume was then determined by optical interferometry (ZeGage, Zygo Corp.). The Ga$^+$ ion current was measured using a Faraday cup and picoammeter. Knowing the total number of Ga$^+$ ions delivered and the crater volume, we calculated a Zr sputtering yield of 3.62 ± 0.27. The uncertainty is expressed as one standard deviation of the five measurements.

In order to determine the quality of the resonance ionization scheme, useful yield measurements are typically done on an ideal surface, such as a surface where all of the Zr

sputters as atoms rather than molecules. Since the top layer of Zr metal accumulates oxygen to form ZrO even at the pressure of our ultra-high vacuum chamber (1×10^{-9} mbar), we pre-sputtered the sample surface prior to every measurement using the Ga$^+$ ion beam at the highest current setting. Pre-sputtering was conducted in an area slightly larger than the measurement area in order to avoid edge effects. We calculated useful yields from surfaces that were pre-cleaned between five and ten minutes, and did not find that the longer cleaning times resulted in more signal. We therefore conclude that a cleaning time of five minutes was long enough to reach a steady-state condition in which the ZrO fraction is minimized. This is analogous to previous studies [6, 10, 12]. The maximum useful yield determined for our selected resonance ionization scheme under these sputtering conditions is $(5.4 \pm 0.4)\%$.

The useful yield of Zr is significantly lower than the 38% measured for U on the same instrument [12]. The mean velocity $\bar{v}$ of sputtered atoms from a metal surface has been demonstrated [13–15] to be:

$$\bar{v} = \frac{4}{\pi} \sqrt{\frac{U_0}{m}} \tag{4}$$

Here, U_0 is the binding energy and m is the mass of the sputtered atom. For a clean Zr surface, the binding energy is 6.3 eV [16, 17]. Using a binding energy of 5.4 eV for U [14, 18, 19], we determine the ratio of average velocities between Zr and U as 1.7. Furthermore, assuming that ion sputtering results in a spherical cloud of atoms with radius r above the sample, the total volume of the cloud V_c scales as $V_c \propto \bar{v}^3$, since the cloud radius $r \propto \bar{v}$. Assuming the ionization laser is cylindrical and goes through the center of the sputtered atom cloud, the ionization volume V_i scales as $V_i \propto r \propto \bar{v}$. This means that the useful yield between two species should scale as $UY \propto V_i/V_c \propto \bar{v}^{-2}$. Assuming the same instrumental conditions for Zr as U we expect a useful yield for Zr of roughly 13%. This is higher than the 5.4% we measured. This crude comparison shows that much but not all of the difference in useful yield between Zr and U is due to the mass difference between the two species, as shown in Eq. (4). The rest could be due to sputter-initiated population of the low-lying $^3F_3$ and $^3F_4$ electronic states [20], which are not accessed in this resonance scheme. Another possibility that could explain the slightly lower-than-expected useful yield is residual oxygen causing formation of ZrO in the sputtered material. Our useful yield measurements show a small peak at m/z 106 (^{90}Zr^{16}O). The non-resonance ionization of ZrO is likely orders of magnitude less effective than resonance ionization of Zr. Since the ionization efficiency of ZrO is not easily quantifiable, sputtering of atoms as ZrO instead of Zr could account for a significant part of the difference between the crude estimate and the actually measured useful yield.

Finally, the possibility exists that a fraction of the atoms in the excited $^3G_3$ and AI states decay to other bound electronic states, rather than to Zr^+. Such dark states would not be re-excited by the available photons and would thus represent another potential loss channel. While our newly developed Zr resonance ionization scheme shows a useful yield that is close to the expectations, future work could also investigate the existence of other schemes that could result in an even higher ionization rate.

Pellin and Nicolussi [8] reported a useful yield for their Zr resonance ionization scheme of $> 2\%$. No further details are given on how the useful yield was determined and for which of the presented Zr resonance ionization schemes it applies. The useful yield determined in this work is still more than a factor of two higher than the one in [8], which is likely due to the fact that the LION instrument has an improved mass spectrometer, and therefore a higher transmission, compared with the instrument used by [8].

The useful yield reported here is lower than expected, however it is still significantly higher than that of the most appropriate comparable technique, secondary ion mass spectrometry (SIMS). A useful yield of $\sim 1.5\%$ is reported for Zr using SIMS in a low-resolution mode [21]. Higher resolving power results in significantly lower useful yield, but would not resolve the atomic Mo and Ru interferences with Zr. The combination of useful yield and isobar discrimination makes RIMS the only technique capable of analyzing heavy elements such as Zr in stardust grains.

Conclusions

We present a newly characterized Zr resonance ionization scheme based on two transitions that can be saturated with current generation titanium-sapphire lasers. Ionization of neutral Zr takes place via an AI state above the IP. The AI transition at $\sim 57,035$ cm^{-1} can easily be saturated with a photon irradiance 1.98×10^4 W cm^{-2}. For 15 keV Ga$^+$ sputtering on Zr metal at 60° incidence, we determined a Zr sputtering yield of 3.62 ± 0.27 using optical interferometry. Combined with resonance ionization mass spectrometry measurements, we showed that the Zr resonance ionization scheme yields an overall useful yield of $(5.4 \pm 0.4)\%$. Previous studies have shown Zr concentrations in presolar SiC grains of up to around 1‰ by weight [22]. Assuming a presolar grain with 1 μm diameter and this given concentration, we can expect that the grain contains a total of around 10^7 atoms of Zr. Assuming the measured useful yield, our new resonance ionization scheme should allow us to measure a $^{96}Zr/^{94}Zr$ isotope ratio to a precision of around 1%, which would be an order of magnitude better than previous work [3]. Since ^{96}Zr can only be reached in AGB nucleosynthesis if the unstable ^{95}Zr is efficiently branched, such

presolar grain measurements will allow us to determine the neutron exposure conditions during the *s*-process in asymptotic giant branch star.

References

1. Nittler LR, Ciesla F (2016) Astrophysics with extraterrestrial materials. Annu Rev Astron Astrophys 54:53–93
2. Nicolussi GK, Davis AM, Pellin MJ, Lewis RS, Clayton RN, Amari S (1997) S-process zirconium in presolar silicon carbide grains. Science 277:1281–1284
3. Barzyk JG, Savina MR, Davis AM, Gallino R, Gyngard F, Amari S, Zinner E, Pellin MJ, Lewis RS, Clayton RN (2007) Constraining the ^{13}C neutron source in AGB stars through isotopic analysis of trace elements in presolar SiC. Meteorit Planet Sci 42:1103–1119
4. Liu N, Gallino R, Bisterzo S, Davis AM, Savina MR, Pellin MJ (2014) The ^{13}C-pocket structure in AGB models: constraints from zirconium isotope abundances in single mainstream SiC grains. Astrophys J 788:163
5. Savina MR, Trappitsch R (2021) In: Zimmermann R, Hanley L (eds) Photoionization and photo-iduced processes in mass spectrometry. Wiley-VCH. https://www.wiley.com/enus/Photoionization+and+Photo+Induced+Processes+in+Mass+Spectrometry%3A+Fundamentals+and+Applicationsp-9783527682225
6. Savina MR, Isselhardt BH, Kucher A, Trappitsch R, King BV, Ruddle D, Gopal R, Hutcheon I (2017) High useful yield and isotopic analysis of uranium by resonance ionization mass spectrometry. Anal Chem 89:6224–6231
7. Moore CE (1952) Atomic energy levels as derived from the analysis of optical spectra—chromium through niobium. The National Bureau of Standards, USA
8. Pellin M J, Nicolussi G K (1998) Trace isotopic analysis of micron-sized grains: Mo and Zr analysis of stardust (SiC and graphite grains) Trace isotopic analysis of micron-sized grains: Mo and Zr analysis of stardust (SiC and graphite grains). In: Proceeding SPIE 3270, Methods for Ultrasensitive Detect, vol. 3270, pp. 148–157
9. Savina MR, Trappitsch R, Isselhardt BH (2018) Electronic excitation of uranium atoms sputtered from uranium metal and oxides. Spectrochim Acta Part B At Spectrosc 149:214–221

10. Trappitsch R, Savina MR, Isselhardt BH (2018) Resonance ionization of titanium: high useful yield and new autoionizing states. J Anal At Spectrom 33:1962–1969

11. Letokhov VS (1977) Laser laser photoionization spectroscopy, vol 584. Acad Press Inc., Cambridge, p 1240

12. Savina MR, Trappitsch R, Kucher A, Isselhardt BH (2018) New resonance ionization mass spectrometry scheme for improved uranium analysis. Anal Chem 90:10551–10558

13. Hintz E, Rusbüldt D, Schweer B, Bohdansky J, Roth J, Martinelli A (1980) The determination of the flux density of sputtered atoms by means of pulsed dye laser excited fluorescence. J Nucl Mater 93–94:656–663

14. Wright R, Pellin M, Gruen D, Young C (1980) Laser fluorescence spectroscopy of sputtered uranium atoms. Nucl Instrum Methods. 170:295–302

15. Bay H, Schweer B, Bogen P, Hintz E (1982) Investigation of light-ion sputtering of titanium using laser-induced fluorescence. J Nucl Mater 111–112:732–737

16. Betz G, Husinsky W (1986) Sputtering of metal targets under increased oxygen partial pressure. Nucl Instrum Methods Phys Res B 13:343–347

17. Brown PL, Curti E, Grambow B, Ekberg C (2005) Chemical thermodynamics of zirconium. Elsevier, Amsterdam

18. Young CE, Cohen RB, Dehmer PM, Pobo LG, Wexler S (1976) Survey of chemi-ionization reactions in accelerated atom–O_2 crossed-molecular beams. J Chem Phys 65:2562–2567

19. Weller RA, Tombrello TA (1978) Energy spectrum of sputtered uranium–a new technique. Radiat Eff 37:83–92

20. Sansonetti JE, Martin WC (2005) Handbook of basic atomic spectroscopic data. J Phys Chem Ref Data 34:1559–2259

21. Hervig RL, Mazdab FK, Williams P, Guan Y, Huss GR, Leshin LA (2006) Useful ion yields for cameca IMS 3f and 6f SIMS: limits on quantitative analysis. Chem Geol 227(1–2):83–99

22. Amari S, Hoppe P, Zinner E, Lewis RS (1995) Trace-element concentrations in single circumstellar silicon carbide grains from the Murchison meteorite. Meteoritics 30:679–693

Publisher's Note Springer Nature remains neutral with regard to jurisdictional claims in published maps and institutional affiliations.